Accepted Manuscript

Metabolomics facilitates the discrimination of the specific anti-cancer effects of free- and polymer-conjugated doxorubicin in breast cancer models

Ana Armiñán, Martina Palomino-Schätzlein, Coralie Deladriere, Juan J. Arroyo-Crespo, Sonia Vicente-Ruiz, María Jesús Vicent, Antonio Pineda-Lucena

PII: S0142-9612(18)30093-0

DOI: 10.1016/j.biomaterials.2018.02.015

Reference: JBMT 18488

To appear in: *Biomaterials*

Received Date: 3 November 2017

Revised Date: 31 January 2018

Accepted Date: 7 February 2018

Please cite this article as: Armiñán A, Palomino-Schätzlein M, Deladriere C, Arroyo-Crespo JJ, Vicente-Ruiz S, Vicent MaríJesú, Pineda-Lucena A, Metabolomics facilitates the discrimination of the specific anti-cancer effects of free- and polymer-conjugated doxorubicin in breast cancer models, *Biomaterials* (2018), doi: 10.1016/j.biomaterials.2018.02.015.

Metabolomics facilitates the discrimination of the specific anti-cancer effects of free- and polymer-conjugated doxorubicin in breast cancer models

Ana Armiñán[a], Martina Palomino-Schätzlein[b], Coralie Deladriere[a], Juan J. Arroyo-Crespo[a], Sonia Vicente-Ruiz[a], María Jesús Vicent[a,**], Antonio Pineda-Lucena[b,c,*]

[a] Polymer Therapeutics Laboratory, Centro de Investigación Príncipe Felipe, Valencia, Spain.
[b] Joint Research Unit in Clinical Metabolomics, Centro de Investigación Príncipe Felipe / Instituto de Investigación Sanitaria La Fe, Valencia, Spain.
[c] Drug Discovery Unit, Instituto de Investigación Sanitaria La Fe, Valencia, Spain.

A. Armiñan and M. Palomino-Schätzlein contributed equally to this article.

***** Corresponding author: Instituto de Investigación Sanitaria La Fe, Avda. Fernando Abril Martorell, 106, 46026-Valencia, Spain. Phone: 34-96-124-6600
** Corresponding author: Centro de Investigación Príncipe Felipe, Avda. Eduardo Primo Yúfera 3, 46012-Valencia, Spain.
Email addresses: pineda_ant@gva.es (A. Pineda-Lucena), mjvicent@cipf.es (M.J. Vicent)

Abstract

Metabolomics is becoming a relevant tool for understanding the molecular mechanisms involved in the response to new drug delivery systems. The applicability of this experimental approach to cell cultures and animal models makes metabolomics a useful tool for establishing direct connections between *in vitro* and *in vivo* data, thus providing a reliable platform for the characterization of chemotherapeutic agents. Herein, we used metabolomic profiles based on nuclear magnetic resonance (NMR) spectroscopy to evaluate the biochemical pathways involved in the response to a chemotherapeutic anthracycline drug (Doxorubicin, Dox) and an N-(2-hydroxypropyl) methacrylamide (HPMA) copolymer-conjugated form (HPMA-Dox) in an *in vitro* cell culture model and an *in vivo* orthotopic breast cancer model. We also used protein expression and flow cytometry studies to obtain a better coverage of the biochemical alterations associated with the administration of these compounds. The overall analysis revealed that polymer conjugation leads to increased apoptosis, reduced glycolysis, and reduced levels of phospholipids when compared to the free chemotherapeutic drug. Our results represent a first step in the application of integrated *in vitro* and *in vivo* metabolomic studies to the evaluation of drug delivery systems.

Keywords: metabolomics, NMR, nanomedicine, polymer therapeutics, breast cancer

Introduction

Chemotherapeutic agents are commonly used to eradicate malignant cells based on their toxicity and/or their ability to prevent cancer cell growth by stopping nutrient uptake or inhibiting cell division. However, non-target tissue toxicity and drug resistance curtails the utility of these agents [1]. For these reasons, the development of new chemotherapeutic agents or site-specific delivery systems is essential for the continued clinical implementation of these therapeutic strategies [1, 2]. In this context, nanomedicine represents a rapidly evolving field that has contributed to enhanced treatment strategies by enabling site-specific release of chemotherapeutic agents [1, 3]. More than 50 different nanomedicines are currently in routine clinical use, and more than 75 anticancer nanomedicine clinical trials are currently ongoing [1, 2]. Polymer therapeutics are considered one of the most successful first generation polymeric nanomedicines [1, 4] and two appear within the US Top 10 selling drugs [4]. Improvements in the development of novel anti-cancer therapeutics are associated with the prolongation of the drug circulation time in blood and the promotion of passive drug tumor accumulation via the enhanced permeability and retention (EPR) effect [5, 6].

The N-(2-hydroxypropyl) methacrylamide (HPMA)–Doxorubicin (Dox) conjugate PK1, also termed FCE28068, was the first synthetic polymer conjugate to enter Phase I trials in 1994 [7]. Over the following years, 22 more polymer-drug conjugates and 2 gamma camera probes have been transferred to the clinic with one conjugate already approved (Movantik®) [8]. Phase I clinical trials with the HPMA copolymer-Dox conjugate revealed the benefits of chemotherapeutic drug conjugation with improved safety and pharmacokinetic profiles [7]. Comparisons with free Dox revealed a higher maximum tolerated dose (MTD) and a lack of polymer-related toxicity, immunogenicity, and, importantly, Dox-related cardiotoxicity [9]. Additionally, polymer conjugation prolongs plasma circulation, inhibits liver accumulation, and enhances renal elimination for the drug-conjugate, thus leading to enhanced responses in metastatic and multidrug resistant breast cancer and non-small cell lung cancer patients [10]. Clinical trials have suggested that patient stratification by specific biomarkers could greatly enhance therapeutic outputs and accelerate approval of advanced therapeutics [11, 12]. Although biomarkers have been already identified, including cathepsin B levels (the enzyme that triggers Dox release from HPMA copolymer) or the state of the tumor vasculature (an important factor for EPR-mediated tumor targeting), the field still requires additional novel functional biomarkers to predict clinical performance.

Metabolomics profiling, an experimental approach focused on the high-throughput identification, quantification and characterization of small molecule metabolites, provides a very

powerful tool for the classification of metabolic phenotypes, the investigation of the physiological status, and the discovery of clinically relevant biomarkers (diagnosis, prognosis, prediction) [13]. Furthermore, metabolomics can contribute to the global evaluation and understanding of the biological effects of new drug delivery systems through the examination of drug-induced metabolic pathways [14] both *in vivo* and *in vitro*. In this context, nuclear magnetic resonance (NMR) spectroscopy represents a fast, effective, and non-destructive method used to obtain structural and quantitative information from metabolic profiles [15]. This analytical platform facilitates the biochemical interpretation of alterations associated with different clinical or pharmacological processes through the analysis of a wide range of biofluids and small molecules.

In this study, we have evaluated the potential of metabolomics to delineate the *in vivo* and *in vitro* response to free Dox and HPMA-Dox in two different breast cancer models. To this end, we obtained NMR metabolomic fingerprints in combination with protein expression and cell cycle profiles from breast cancer cell cultures and an orthotopic immunocompetent breast tumor animal model following treatment with free- and polymer-conjugated Dox. Our data support an enhanced anti-cancer activity of the conjugate over the free drug and positively correlate with clinical observations regarding toxicological and pharmacokinetic profiles of both compounds [7].

Materials and Methods

Synthesis of HPMA copolymer-Dox conjugate

The Dox conjugation reaction was performed according to a previously described procedure [16] (Supplementary Scheme S1).

Cell culture conditions

The MCF7 breast adenocarcinoma cell line was grown in Dulbecco's Modified Eagle Medium (DMEM) with 4500 mg glucose /L (Sigma Aldrich) supplemented with 10% v/v fetal bovine serum (FBS) at 37°C in 5% carbon dioxide and 95% air. Cells underwent passage once weekly. The 4T1 cell line was grown in RPMI 1640 Medium (Thermo Fisher) supplemented with 10% v/v FBS at 37°C in 5% carbon dioxide and 95% air. Cells underwent passage twice a week.

Cell culture and harvesting for metabolomics

MCF7 cells were cultured in P150 plates at 25,000 cells/cm^2. After 24 h incubation, cells were treated with HPMA-Dox or free Dox at concentrations of 0.75 µg/ml and 7.5 µg/ml Dox equiv., respectively, for 72h. Medium was then collected and centrifuged at 400 g for 7 min to collect cell free conditioned medium, while the remaining pellet, corresponding to cells that had detached during treatment, was washed with PBS and stored at 4ºC. In parallel, cells attached on the plate were washed twice with 10 ml of PBS, collected, and added to the corresponding previously collected pellet. Finally, 160 µL of methanol were added to the final pellets and frozen with liquid nitrogen and stored at -80ºC.

Annexin V assay and cell cycle studies

Cells were seeded at a density of 25,000 cells/cm^2 in sterile P35 plates. After 24 hours of incubation, cells were treated for 72h with HPMA-Dox or free Dox at a concentration of 7.5 µg/ml Dox equiv, the IC50 of HPMA-Dox. The experiments were carried out in triplicate and untreated cells were used as control (Ctr).

Annexin V Assay: Apoptosis was quantified by flow cytometry using Annexin V. Cells were labeled with Annexin V-FITC (Immunostep S.L.) following the manufacturer's instructions. Samples were analyzed by flow cytometry using a Cytomics FC 500 (Beckman Coulter Inc.) equipped with an air cooled argon ion laser (488 nm, 15 mV) and the fluorescence emission was appropriately filtered at green wavelength (525 nm). Data collection involved 10,000 counts per sample.

Cell Cycle Studies: Cells were fixed with 70% ethanol overnight at -20ºC and labeled with 500 µl of propidium iodide (PI) solution (50 µg/ml of PI and 50 µg/ml of RNAase in PBS) in the

dark at room temperature for 60 min. The DNA content of cells was analyzed using a flow cytometer (Cytomics FC 500, Beckman Coulter Inc.). Data was analyzed by WinMDI 2.9 and Cylchred software.

4T1 orthotopic breast tumor animal model

Animal experiments were performed in accordance with the guidelines established by the European Communities Council Directive (86/609/ECC) and by Spanish Royal Decree 1201/2005. The institutional Animal Care and Use Committee approved all the experimental procedures.

4-6 week-old Balb/c female mice purchased from Harlan Laboratories Inc. (Spain, EU) were injected with 5 x 10^5 4T1 mammary carcinoma cells in the right second mammary pad. Tumor growth was followed every two days with a caliper. After 8 days, when the tumor size reached 0.1 cm^3, intravenous treatment was administrated at 3 mg/kg of Dox equiv. three times every three days to evaluate anti-tumor activity. Tumor size and animal weight were measured daily and when the tumor achieved the maximum size authorized (1 cm^3, around 16 days of the treatment starting), tumors were extracted, weighed and frozen for metabolomic and protein expression profile analysis. At least 7 animals were included in each experimental group.

Western blot analysis

MCF7 cells were seeded at a cell density of 25,000 cells/ cm^2 in sterile P60 plates and treated with HPMA-Dox and Dox (7.5 μg/ml Dox equiv.) for 72 hours. Total cellular proteins were extracted with cell lysis buffer (50 mM Tris–HCl pH 8.0, 2 mM NaCl, 1% NP-40, 2% SDS). Tumor samples were homogenized using Ultra-Turrax (IKA®-Werke GmbH & Co. KG, Staufen, Germany, EU) and proteins extracted using RIPA buffer (150 mM NaCl, 1% NP40, 0.5% sodium deoxycholate, 0.1% SDS, 50 mM Tris pH8, 50 mM NaF, 100 μM Na_3VO_4 and 1x protease inhibitor cocktail). Protein content was quantified by Bradford assay and 20 μg of protein extract was used to study the expression of caspase 3, LC3II, pAkt and PARP by western blotting. The primary antibodies anti-caspase 3 (1:1,000), anti-Beclin1 (1:200), anti-LC3II (1:500) and anti-pAkt (1:750) were purchased from Cell Signaling; antibody anti-PARP (1:500) was purchased from Abcam and α-tubulin (1:5,000) from Sigma Aldrich.

Measurement of reactive oxygen species (ROS)

Reactive oxygen species (ROS) levels were determined using the fluorescent marker 2′,7′-dichlorodihydrofluorescein diacetate (DCFH-DA) [17]. DCFH-DA enters the cell and after oxidation by ROS, it is transformed into the highly fluorescent 2',7'-dichlorofluorescein (DCF). Briefly, after treatment with HPMA-Dox and Dox, cells were trypsinized and incubated with 5

µg/ml DCFH-DA (Sigma-Aldrich, Inc) for 30 min in the dark. The number of positive cells and the intensity of fluorescence were then measured by flow cytometry using a Cytomics FC 500 (Beckman Coulter Inc).

Metabolomic analysis

Metabolites were subsequently extracted from cell pellets and frozen tumor tissues, using the chloroform-methanol-water protocol [18]. Details on metabolite extraction and sample preparation, NMR spectroscopy, data processing, and analysis are described in the Supplementary Data section.

Statistical analysis

Data from *in vitro* studies are reported as the mean ± SEM of at least three independent experiments. *In vivo* experiment results are expressed as mean ± SEM with at least n = 7 samples per group. Statistical analysis was performed using one-way ANOVA test and Mann–Whitney U test; comparisons with $p<0.05$ were considered statistically significant with a 95% confidence interval. Further details regarding the statistical analysis of the metabolomics data are included in the Supplementary Data section.

Results

In vitro study of free and polymer-conjugated Dox

Dose calculation

We determined the optimal doses of free Dox and HPMA-Dox for the study based on the cytotoxicity of the polymer-drug conjugate and the free drug in MCF7 cells under the experimental conditions (Supplementary Fig. S1). The MTS assay provided an IC50 of 7.5 µg/ml Dox equiv. for HPMA-Dox and 5.2 µg/ml for Dox after 72 hours of treatment. To compare the same drug equiv. for both treatments, we used the IC50 of HPMA-Dox as a working concentration for both the free and the conjugated drug. Cell counts together with a clonogenic assay showed the cytotoxic effect of both compounds and the absence of survival response in MCF7 cells following the induction of cell death, confirming the anti-cancer effect of HPMA-Dox (Supplementary Fig. S2). For low dose studies, we used 0.75 µg/ml Dox-equiv. as a non-toxic concentration.

Metabolomic profiles

Using NMR spectroscopy, we obtained metabolomic profiles of the aqueous (polar) and organic (non-polar) phases from MCF7 cells exposed to free Dox and HPMA-Dox. Fig. 1A depicts representative ^{1}H-NMR spectra of polar metabolites obtained from aqueous phases under different cell culture conditions. NMR spectra obtained for non-polar metabolites corresponding to the associated organic phases can be found in the Supplementary Data (Supplementary Fig. S3). Access to a sensitivity-enhanced NMR cold probe allowed the acquisition of high quality spectra and the identification and quantification of 35 different intracellular metabolites (Supplementary Tables S1 and S2). The analysis of the metabolites present in the cell culture medium led to the identification and quantification of 14 metabolites, including amino acids, organic acids, and sugars (Supplementary Table S3).

We characterized metabolic alterations after treatment using principal component analysis (PCA) and, as shown in Fig. 1B, the different samples grouped according to the specific treatment. A detailed analysis of the corresponding loadings plot (Supplementary Fig. S4) and the relative concentrations of the assigned metabolites (Supplementary Fig. S5) allowed the identification of the compounds responsible for the discrimination between the different groups. Fig. 1B summarizes the main metabolite variations associated with the treatment. Specific details can be found in Supplementary Fig. S5.

Data analysis revealed the existence of specific metabolic alterations differentiating the activity of free Dox and HPMA-Dox. MCF7 cells exposed to free Dox experienced a specific increase in the levels of lactate, myo-inositol, glutamine, and glucose, and decreased levels of

glutamate, glycine, acetate, phosphocholine (PC), nicotinamide adenine dinucleotide (NAD+), and glutathione (GSH), while HPMA-Dox treated cells displayed increased creatine and phosphocreatine levels and decreased glutamine levels. Several metabolites, including alanine, adenosine triphosphate (ATP), aspartate, glycerophosphocholine (GPC), isoleucine, valine, and leucine experienced a similar change in the presence of both drugs (Fig. 1B and Supplementary Fig. S5), although free Dox induced a more pronounced effect.

Analysis of the organic phase (non-polar metabolites) in the presence of free Dox revealed a decrease in the levels of phospholipids, fatty esters, and cholesterol in the presence of the free drug, and an increase of polyunsaturated fatty acids (PUFA) and triacylglicerides (TAG) (Supplementary Fig. S5). Overall, treatment with HPMA-Dox induced similar, although less pronounced, changes in the lipid profile of MCF7 cells, with the exception of a decrease in the TAG levels. Fig. 2 displays the metabolites exhibiting the most significant changes, and Supplementary Fig. S5 summarizes all the identified alterations.

The analysis of the metabolic profiles corresponding to the cell content provides very valuable information on the metabolic routes undergoing alterations in the presence of the different treatments. However, it does not properly inform on the specific metabolic exchanges between the cells and the cell culture medium. Thus, in order to get a better understanding of the modifications affecting extracellular metabolites, the metabolic profile of the cell culture medium was also analyzed at 0 h *vs* 72 h (Supplementary Fig. S6). Results revealed a decrease in the levels of most amino acids, choline, phosphocholine and glucose, metabolites that are uptaken by the cell, and an increase in lactate due to anaerobic processes. As expected from their pharmacological activity, treatment with Dox or HPMA-Dox led to a reduction of these changes. In general, we observed no differences when comparing both treatments, with the exception of an increase in histidine levels after HPMA-Dox treatment.

Flow cytometry study

In order to get a better understanding of the biological effects induced by free and conjugated Dox, we employed flow cytometry analysis to evaluate apoptosis following treatment with both drugs. As shown in Fig. 2G, we detected apoptotic cells in both cases, although the induction of this process was significantly more pronounced in the presence of free Dox (20 ± 2 %) compared to HPMA-Dox (11 ± 3 %).

Reactive oxygen species (ROS) generation is a well-known process involved in Dox-associated cardiotoxicity [19]. Therefore, to quantify the amount of oxidative stress in treated cells, we measured ROS levels with 2',7'-dichlorfluorescein-diacetate (DCFH-DA), a sensitive oxidative stress fluorometric probe for living cells [17]. As shown in Fig. 2H, incubation of MCF7 cells with

Dox caused a significant (4.47 ± 0.41 fold) increase in DCF fluorescence compared to untreated cells (Ctr) ($p<0.005$), or cells treated with HPMA-Dox (2.13 ± 0.29 fold; $p< 0.01$). We confirmed these results using an OxiSelect Intracellular ROS Assay Kit (data not shown).

Cell cycle analysis by flow cytometry revealed significant differences in the proportion of cells in G0/G1, S, and G2/M when comparing the drug-treated groups with the control group (Fig. 2I). Thus, free Dox treatment led to a decreased percentage of cells in G0/G1 and G2/M phases, as well as to an increase in S phase content, indicative of an S phase cell cycle arrest. HPMA-Dox treatment also decreased the percentage of cells in G0/G1 phase. However, in this case, the percentage of cells in G2/M and S phases increased, suggesting the induction of cell cycle arrest at G2/M phase (Fig. 2I). In this context, the expression of the cyclin-dependent kinase inhibitor p21, a protein directly involved in G2/M cell cycle arrest, provided further evidence of this process in cells exposed to the HPMA-Dox conjugate (Fig. 2J).

Protein expression profiles

Further analysis of the MCF7 cell cultures revealed that treatment with both Dox and HPMA-Dox led to a significant increase, compared to untreated cells, in the DNA damage repair protein poly(ADP-ribose) polymerase (PARP-1) **(**Fig. 2K). However, expression of PARP-1 was significantly higher in the presence of Dox, thus suggesting a reduction of DNA damage in HPMA-Dox treated cells. Evaluation of autophagy-related proteins (Beclin 1 and LC3II) revealed a significant increase in the expression of these proteins after drug treatment, particularly for HPMA-Dox treated cells (Fig. 2L). However, we did not observe any evidence of a survival response in MCF7 cells following the induction of autophagy, confirming the anti-cancer effect of HPMA-Dox (Supplementary Fig. S2B).

***In vivo* study of free and polymer-conjugated Dox**

Dose calculation and time points

To further characterize the molecular mechanisms involved in the response to both drugs, we employed an *in vivo* 4T1 orthotopic breast tumor mouse model, with doses previously optimized to guarantee animal survival [20]. Once tumors reached the maximum permitted size, we collected samples for metabolomics and protein expression profile analyses. Although treatments had no effect on the body weight of the animals (Supplementary Fig. S7), treatment with HPMA-Dox led to a significant reduction in tumor growth compared to free Dox treated or control animals (Fig. 3A).

Metabolomic profiles

Fig. 3B displays representative ^{1}H NMR spectra of the aqueous phase of breast tumor extracts from control, free Dox and HPMA-Dox treated mice. The corresponding spectra of the organic phase can be found in the Supplementary Data (Supplementary Fig. S8). We identified and quantified a total of 45 different intracellular metabolites using NMR approaches, as summarized in Supplementary Tables S4 and S5.

To discriminate metabolic differences induced by the treatment with both drugs from the inter-individual variability between animals, we applied a supervised multivariate statistical analysis, Orthogonal Partial Least Squares Regression Discriminant Analysis (OPLS-DA). The resulting score plot (Fig. 3C) revealed that samples grouped according to the specific treatment. To get a better understanding of the specific metabolic alterations induced by each treatment, we generated two different OPLS-DA models (free-Dox treated *vs* control mice, HPMA-Dox treated *vs* control mice) **(**Supplementary Figs. S9 and S10).

Multivariate statistical results revealed that the first model (free-Dox treated *vs* control mice) exhibited a modest discriminatory power (R^2 = 0.68, Q^2 = 0.15) However, samples from the HPMA-Dox treated mice could be clearly discriminated from control mice with high R^2 (0.88) and Q^2 (0.74) values, suggesting a more reliable model.

Fig. 4A-C illustrates the most significant metabolite variations between groups obtained after the analysis of the corresponding S-plots (Supplementary Figs. S9 and S10) and integration of metabolic regions (Supplementary Fig. S11). We observed several common changes in polar metabolites for both treatments, such as increased PC and glucose levels, and decreased glutamate, GPC, and myo-inositol levels. However, many other changes, including increased levels of cytidine, lysine, and uridine diphosphate (UDP) derivatives, and decreased phosphocreatine and glycine were only observed in the HPMA-Dox treated group (Fig. 4A-B and Supplementary Fig. S11). As for the non-polar metabolites, we did not detect statistically significant variations for the samples collected from free-Dox treated mice compared to control mice. On the contrary, we observed significant changes for HPMA-Dox treated mice, characterized by decreased levels of phospholipids and unsaturated lipids, and increased levels of cholesterol as compared to control mice (Fig. 4C).

Protein expression profiles

To further characterize the effects of both drugs in the animal model, we evaluated the expression of proteins involved in different molecular processes. Using this approach, we discovered a decrease in pAkt levels in tumor lysates [21] following both treatments (Fig. 4D), and

a significant increase in caspase-3 only after HPMA-Dox treatment (Fig. 4E). However, we did not observe significant changes in the levels of the autophagic protein LC3II (data not shown).

Discussion

In this study, we evaluated the biochemical alterations induced by Dox, and anticancer therapeutic, and a polymer conjugate derived from this drug, HPMA-Dox, in MCF7 cells as well as in an orthotopic immunocompetent animal model recapitulating the characteristic features of breast cancer. We pursued an experimental approach relying on the analysis of metabolomic and protein expression profiles, as well as on flow cytometry studies, to achieve a better understanding of the molecular processes involved in the biological response to both chemotherapeutic agents, and the benefits of administering polymer conjugates over free agents.

The *in vitro* study provided relevant information regarding the changes induced by both drugs at different levels. We found that MCF7 cells exposed to these compounds experience significant changes in their bioenergetics. Most of the alterations identified after treatment with free Dox and HPMA-Dox had a very similar trend, although those associated with the latter were, in general, less pronounced. The reduced magnitude of the biochemical alterations induced by HPMA-Dox could be related to the lysosomotropic intracellular delivery of this agent, that leads to a sustained and slower intracellular Dox release, clearly contrasting with the random cell diffusion characteristic of free Dox [22].

In this context, the decreased glucose consumption (Supplementary Fig. S6), with the concomitant elevation of glucose levels inside the cells (Figs. 2A and 4A), as well as the increased lactate production (Supplementary Fig. S6), tend to suggest a reduction of the glycolytic rate. This is exactly the opposite behavior found in neoplastic cells, that are characterized by an increased glucose consumption and a reduced free glucose content [23]. Moreover, the decreased levels of glutamate and glycine (Fig. 2A) have been linked to a reduction of glycolysis [24], and glycine, in particular, has been proposed as a biomarker for cancer prognosis and treatment response [25]. Furthermore, the reduced fumarate levels could indicate an activation of the mitochondrial energy production pathway in detriment of anaerobic process by Dox and HPMA-Dox (Fig. 2F), a process that would activate prolyl hydroxylase domain (PHD) enzymes as it has been suggested in recent studies [26]. A reduction of glutaminolysis and glucose consumption could also be involved in the observed decrease of glutamate levels, and those of alanine and aspartate (Fig. 2B), two amino acids that are generated from glutamine [27]. Glutaminolysis is a biochemical process, responsible for the conversion of glutamine into glutamate to provide anaplerotic carbons through the TCA cycle [28], that plays an important role in the survival and proliferation of cancer cells under hypoxic and low glucose conditions [29]. Therefore, it should be expected that treatment of MCF7 cells with chemotherapeutic agents will have an important impact in glutaminolysis.

MCF7 cells exposed to free Dox also exhibited significant changes in lipid metabolism (Fig. 2D). In contrast, we did not observe significant phospholipid changes after treatment with HPMA-

Dox (Fig. 2D). Many preclinical and clinical studies have reported higher phospholipid levels when comparing cancer and normal tissues [30], perhaps reflecting the increased cell membrane synthesis required for tumor cell replication [31]. Furthermore, many studies have documented the severe reduction in phospholipid levels in response to different chemotherapeutic regimes [32, 33], thus supporting our own findings. Alterations of the phospholipid synthesis could be associated with the different cell cycle profiles induced by free Dox and HPMA-Dox [34] and studies have reported that MCF7 cells exhibit increased rates of phospholipids synthesis in G2/M and early G1 phases [34]. This observation is in agreement with our experimental results, and would explain why MCF7 cells exposed to free Dox, which induces cell cycle arrest in S phase, show decreased phospholipid levels. On the contrary, treatment with HPMA-Dox, that arrests MCF7 cells in the G2/M phase, as was confirmed in our study by the specific induction of p21 (Fig. 2J), does not induce significant changes in the phospholipid profile when compared with untreated cells (Fig. 2I).

Oxidative stress, a disturbance in the balance between the production of ROS and antioxidant defenses that can lead to mitochondrial alterations and apoptosis, is accompanied by a number of metabolic alterations. In this context, our results (Fig. 2H) support previous studies suggesting that free Dox could be a significant inductor of oxidative stress [19, 35]. To this end, we note that metabolic alterations associated with this process include a reduction of GSH levels, considered a biomarker of oxidative stress in treated cancer cells [36], as well as an upregulation of leucine [37] and the downregulation of glycine and ATP [38], processes that have been linked to oxidative stress-induced senescence. Furthermore, it seems there is also a connection between a reduction in NAD+ levels and the induction of oxidative stress, as derived from some breast cancer studies [36]. As shown in Fig. 2E, the biochemical alterations induced by free Dox in MCF7 cells are in perfect agreement with the characteristic metabolic features associated with oxidative stress, and could also be related to changes in lipid metabolism. However, treatment of MCF7 cells with HPMA-Dox did not induce significant changes in the levels of those metabolites, indicating that oxidative stress does not play a significant role in its mode of action. This conclusion is further supported by the fact that similar rates of cell growth were found for free Dox and HPMA-Dox treated cells in our study, suggesting that oxidative stress may not interfere in the proliferation of MCF7 cells in these conditions, as it was previously observed for cisplatin and anthracyclines [39]. Instead, ROS generation may mediate anthracycline-induced cardiotoxicity [39, 40], liver toxicity [41], cutaneous drug reaction [42], and kidney toxicity [19]. In this context, polymer conjugation of anthracyclines, as already demonstrated in the clinics with PK1 (HPMA-Dox conjugate) [6, 9] and also in preclinical models developed by us [20] and others [43], limits toxic side effects by facilitating tumor accumulation of the drug based on the EPR effect and the different biodistribution diminishing Dox cardiac accumulation.

Finally, oxidative damage induced by cytotoxic agents can lead to the hyperactivation of PARP-1, a DNA binding enzyme activated by DNA breaks and involved in DNA repair, genomic stability, transcriptional control, cell death and proliferation [44]. Activation of PARP-1 by DNA strand breaks results in the synthesis of poly(ADP-ribose) at the expense of NAD+. Our results also show a significant overexpression of PARP-1 in MCF7 cells after treatment with free Dox (Fig. 2K), suggesting that DNA damage induced by this compound could be responsible for the induction of this protein and the reduction of the NAD+ levels.

Flow cytometry studies, based on Annexin V-FITC staining, revealed that, in addition to metabolic changes, treatment of MCF7 cells with free Dox, and in a lesser extent with HPMA-Dox, induced apoptosis (Fig. 2G). This process could be a reflection of a reduced energy supply, although a number of studies have reported that apoptosis may not be a critical factor for the effectiveness of treatment with Dox [45]. Significant increases in the levels of polyunsaturated lipids (PUFA) have been previously linked to apoptosis induced by cytotoxic agents [36, 46], and they could reflect alterations in the membrane bilayer fluidity [47] or the generation of cytoplasmic lipid droplets [48]. Furthermore, apoptosis seems also to be associated with increased levels of branched amino acids (valine, leucine, isoleucine) (Fig. 2C) [49], and decreased alanine levels (Fig. 2B) [50].

Treatment of MCF7 cells with HPMA-Dox led to a smaller induction of apoptosis, when compared with free Dox (Fig. 2G), suggesting the presence of alternative cell death mechanisms induced upon polymer conjugation. To this end, our studies revealed a significant increase of LC3II and Beclin1 in MCF7 cells treated with HPMA-Dox as compared to free Dox (Fig. 2L), two proteins that are closely associated with the induction of autophagic processes. Interestingly, autophagy seems to proceed via glutamine metabolism [51], our results showing a specific reduction of this amino acid after treatment with HPMA-Dox, a metabolic alteration that could associated with the induction of this process in MCF7 cells (Fig. 2A). Additional clonogenic experiments performed to study the long-term effect of autophagy revealed that the induction of autophagy caused cell death due to the inhibition of new colony formation (Supplementary Fig. S2B). The induction of this process after treatment with HPMA-Dox could contribute to the modulation of the toxic side effects induced by anthracyclines [52].

We followed the *in vitro* study with an *in vivo* evaluation of the effect of both free Dox and HPMA-Dox in an orthotopic breast tumor mouse model [27]. The evaluation revealed that most of the metabolic changes associated with altered glycolysis (decreased glutamate and glycine, increased glutamine and glucose) were retained in the animal model after treatment with these compounds (Fig. 4A). This metabolic signature could therefore represent a promising biomarker for characterizing cytotoxic effects in future studies. We also confirmed alterations of the glycolytic

metabolism by the observed reduction of pAkt levels (Fig. 4D). The PI3K/Akt pathway is activated by growth factors and plays a very important role in the proliferative behavior of cancer cells. Furthermore, Akt is involved in the expression and membrane localization of the glucose transporter GLUT1, that facilitates the transport of this metabolite across plasma membranes to be metabolized in the cells through a glycolytic mechanism [21].

Changes in the levels of metabolites associated with glycolysis were also accompanied by alterations in the levels of several phospholipids (Fig. 4C), particularly after treatment with HPMA-Dox, thus confirming the implication of these metabolites in the response to chemotherapeutic treatments. Interestingly, while we did not detect evidence of alterations in metabolites associated with apoptosis (increased valine, leucine, isoleucine, PUFA) in the animal model, we did find a significant increase in UDP-GlcNAC, an UDP derivative that has been related to the induction of apoptosis by chemotherapeutic agents [40, 41](Fig. 4B). A significant increase in the expression of the pro-apoptotic protein caspase-3 further confirmed that HPMA-Dox induces apoptotic processes (Fig. 4E). The upregulation of caspase-3 seems also to be correlated with the observed delay in tumor growth after treatment with the polymer conjugate (Fig. 3A). In general, metabolic changes (glycolysis, phospholipid levels, and apoptosis) were much more pronounced for HPMA-Dox than for the free drug, an observation that has a reflection in the reduction of the tumor size obtained in both cases. Therefore, our study suggests that treatment with polymer conjugates induces biochemical alterations that are maintained over longer periods of time compared to the free drug. This observation is in agreement with the clinical data obtained with PK1 (HPMA-Dox) and can be associated with the characteristic pharmacokinetics profile expected for these macromolecular compounds (EPR effect and lysosomotropic delivery [1, 11-12]).

Conclusion

This study represents a first step towards the development of a robust platform for the application of *in vitro* and *in vivo* metabolomics approaches for getting a better understanding of the biochemical alterations induced by free or polymer-conjugated chemotherapeutic agents. *In vitro* experiments using MCF7 cells revealed metabolic alterations that are reflective of the different cellular trafficking of both the free drug (diffusion) and the polymer conjugate (endocytosis and lysosomotropic drug release). Furthermore, the *in vitro* model facilitated the characterization of different biochemical and molecular mechanisms involved in the efficacy and toxicity of both agents. The *in vivo* studies indicated that treatment with HPMA-Dox induced more significant changes than free Dox, reflecting the enhanced pharmacokinetics (elevated blood circulation times) and biodistribution (higher tumor and lower cardiac accumulation) of the polymer conjugate.

Importantly, these studies also facilitated the identification of specific biomarkers (i.e., PUFA, glucose, UDP-NAG, etc.) associated with the pharmacological effect of HPMA-Dox that could be extrapolated to other polymer-anticancer drug conjugates.

In summary, our work shows that metabolomics, in combination with other experimental approaches, could provide a very relevant tool for characterizing the biochemical effects of polymer conjugates, both in terms of efficacy and toxicity. Future translation of these results to the clinics would benefit from the validation of the identified biomarkers in patient liquid biopsies to assess, in a non-invasive manner, treatment performance in cancer patients undergoing therapy based on polymer-anticancer drug conjugates.

Disclosure of Potential Conflicts of Interest

The authors declare no conflict of interest.

Author´s Contributions

Conception and design: A. Armiñán, M. Palomino-Schätzlein, M.J. Vicent, A. Pineda-Lucena
Development of methodology: A. Armiñán, M. Palomino-Schätzlein
Acquisition of data (provided animals, acquired and managed patients, provided facilities, etc.): A. Armiñán, M. Palomino-Schätzlein, C. Deladriere, J.J. Arroyo-Crespo, S. Vicente-Ruiz
Analysis and interpretation of data (e.g., statistical analysis, biostatistics, computational analysis): A. Armiñán, M. Palomino-Schätzlein
Writing, review, and/or revision of the manuscript: A. Armiñán, M. Palomino-Schätzlein, M.J. Vicent, A. Pineda-Lucena
Administrative, technical, or material support (i.e., reporting or organizing data, constructing databases): A. Armiñán, M. Palomino-Schätzlein
Study supervision: M.J. Vicent, A. Pineda-Lucena

Acknowledgements

The authors acknowledge Stuart P. Atkinson for English editing, L. Ortí for her technical support in metabolomics sample preparation, E. Masiá for the technical support in the performance of clonogenic assays and D. Charbonnier for assisting in animal management.

Grant Support

This work was supported by the Centro de Investigación Príncipe Felipe, the Instituto de Investigación Sanitaria La Fe, the Spanish Ministry of Economy and Competitiveness (Grant numbers SAF2013-44848-R, SAF2016-80427-R, SAF2014-53977-R, SAF2017-89229-R) and the European Research Council (Grant number ERC-CoG-2014-648831 [MyNano]).

References

[1] R. Duncan, R. Gaspar, Nanomedicine(s) under the microscope, Mol. Pharm. 8 (2011) 2101-2141.
[2] J.I. Hare, T. Lammers, M.B. Ashford, S. Puri, G. Storm, S.T. Barry, Challenges and strategies in anti-cancer nanomedicine development: An industry perspective, Adv. Drug Deliv. Rev. 108 (2017) 25-38.
[3] D. Landesman-Milo, D. Peer, Transforming Nanomedicines From Lab Scale Production to Novel Clinical Modality, Bioconjug. Chem. 27 (2016) 855-862.
[4] R. Duncan, Polymer therapeutics: Top 10 selling pharmaceuticals — What next?, J. Control. Release. 190 (2014) 371-380.
[5] Y. Matsumura, H. Maeda, A new concept for macromolecular therapeutics in cancer chemotherapy: mechanism of tumoritropic accumulation of proteins and the antitumor agent smancs, Cancer Res. 46 (1986) 6387-6392.
[6] H. Maeda, Polymer therapeutics and the EPR effect, J. Drug Target. 25 (2017) 781-785.
[7] P.A. Vasey, S.B. Kaye, R. Morrison, C. Twelves, P. Wilson, R. Duncan, et al., Phase I clinical and pharmacokinetic study of PK1 [N-(2-hydroxypropyl)methacrylamide copolymer doxorubicin]: first member of a new class of chemotherapeutic agents-drug-polymer conjugates. Cancer Research Campaign Phase I/II Committee, Clin. Cancer Res. 5 (1999) 83-94.
[8] M.J. Vicent, L. Dieudonne, R.J. Carbajo, A. Pineda-Lucena, Polymer conjugates as therapeutics: future trends, challenges and opportunities, Expert Opin. Drug Deliv. 5 (2008) 593-614.
[9] R. Duncan, Development of HPMA copolymer-anticancer conjugates: clinical experience and lessons learnt, Adv. Drug Deliv. Rev. 61 (2009) 1131-1148.
[10] L.W. Seymour, D.R. Ferry, D.J. Kerr, D. Rea, M. Whitlock, R. Poyner, et al., Phase II studies of polymer-doxorubicin (PK1, FCE28068) in the treatment of breast, lung and colorectal cancer, Int. J. Oncol. 34 (2009) 1629-1636.
[11] R. Duncan, Polymer conjugates as anticancer nanomedicines, Nat. Rev. Cancer. 6 (2006) 688-701.
[12] F. Canal, J. Sanchis, M.J. Vicent, Polymer--drug conjugates as nano-sized medicines, Curr. Opin. Biotechnol. 22 (2011) 894-900.
[13] A. Halama, Metabolomics in cell culture--a strategy to study crucial metabolic pathways in cancer development and the response to treatment, Arch. Biochem. Biophys. 564 (2014) 100-109.
[14] J. Carrola, V. Bastos, I. Jarak, R. Oliveira-Silva, E. Malheiro, A.L. Daniel-da-Silva, et al., Metabolomics of silver nanoparticles toxicity in HaCaT cells: structure-activity relationships and role of ionic silver and oxidative stress, Nanotoxicology. 10 (2016) 1105-1117.
[15] J.K. Nicholson, J.C. Lindon, Systems biology: Metabonomics, Nature. 455 (2008) 1054-1056.
[16] M.J. Vicent, F. Greco, R.I. Nicholson, A. Paul, P.C. Griffiths, R. Duncan, Polymer therapeutics designed for a combination therapy of hormone-dependent cancer, Angew. Chem. Int. Ed. Engl. 44 (2005) 4061-4066.
[17] H. Zhu, G.L. Bannenberg, P. Moldeus, H.G. Shertzer, Oxidation pathways for the intracellular probe 2',7'-dichlorofluorescein, Arch. Toxicol. 68 (1994) 582-587.
[18] E. Martineau, I. Tea, G. Loaec, P. Giraudeau, S. Akoka, Strategy for choosing extraction procedures for NMR-based metabolomic analysis of mammalian cells, Anal. Bioanal. Chem. 401 (2011) 2133-2142.
[19] C. Carvalho, R.X. Santos, S. Cardoso, S. Correia, P.J. Oliveira, M.S. Santos, et al., Doxorubicin: the good, the bad and the ugly effect, Curr Med Chem. 16 (2009) 3267-3285.
[20] C. Deladriere, A. Armiñán, E. Masiá, R. Lucas, M.J. Vicent, (2018) In Preparation.
[21] C. Munoz-Pinedo, N. El Mjiyad, J.E. Ricci, Cancer metabolism: current perspectives and future directions, Cell Death Dis. 3 (2012) e248.
[22] F. Greco, M.J. Vicent, S. Gee, A.T. Jones, J. Gee, R.I. Nicholson, et al., Investigating the mechanism of enhanced cytotoxicity of HPMA copolymer–Dox–AGM in breast cancer cells, J Control. Release. 117 (2007) 28-39.

[23] X.M. Zhou, C.C. He, Y.M. Liu, Y. Zhao, D. Zhao, Y. Du, et al., Metabonomic classification and detection of small molecule biomarkers of malignant pleural effusions, Anal. Bioanal. Chem. 404 (2012) 3123-3133.
[24] Y. Yang, C. Li, X. Nie, X. Feng, W. Chen, Y. Yue, et al., Metabonomic studies of human hepatocellular carcinoma using high-resolution magic-angle spinning 1H NMR spectroscopy in conjunction with multivariate data analysis, J. Proteome Res. 6 (2007) 2605-2614.
[25] L. Mirbahai, M. Wilson, C.S. Shaw, C. McConville, R.D. Malcomson, J.L. Griffin, et al., 1H magnetic resonance spectroscopy metabolites as biomarkers for cell cycle arrest and cell death in rat glioma cells, Int. J. Biochem. Cell Biol. 43 (2011) 990-1001.
[26] P. Esteves, C. Pecqueur, C. Ransy, C. Esnous, V. Lenoir, F. Bouillaud, et al., Mitochondrial retrograde signaling mediated by UCP2 inhibits cancer cell proliferation and tumorigenesis, Cancer Res. 74 (2014) 3971-3982.
[27] I.K. Straadt, J.F. Young, B.O. Petersen, J.O. Duus, N. Gregersen, P. Bross, et al., Oxidative stress-induced metabolic changes in mouse C2C12 myotubes studied with high-resolution 13C, 1H, and 31P NMR spectroscopy, J. Agric. Food Chem. 58 (2010) 1918-1926.
[28] P. Tripathi, P. Kamarajan, B.S. Somashekar, N. MacKinnon, A.M. Chinnaiyan, Y.L. Kapila, et al., Delineating metabolic signatures of head and neck squamous cell carcinoma: phospholipase A2, a potential therapeutic target, Int. J. Biochem. Cell Biol. 44 (2012) 1852-1861.
[29] N.E. Simpson, V.P. Tryndyak, F.A. Beland, I.P. Pogribny, An in vitro investigation of metabolically sensitive biomarkers in breast cancer progression, Breast Cancer Res. Treat. 133 (2012) 959-968.
[30] E. Ackerstaff, K. Glunde, Z.M. Bhujwalla, Choline phospholipid metabolism: a target in cancer cells?, J. Cell Biochem. 90 (2003) 525-533.
[31] J. Ruiz-Cabello, J.S. Cohen, Phospholipid metabolites as indicators of cancer cell function, NMR Biomed. 5 (1992) 226-233.
[32] O.M. Redmond, J.P. Stack, N.G. O'Connor, D.N. Carney, P.A. Dervan, B.J. Hurson, et al., 31P MRS as an early prognostic indicator of patient response to chemotherapy, Magn. Reson. Med. 25 (1992) 30-44.
[33] J.M. Maris, A.E. Evans, A.C. McLaughlin, G.J. D'Angio, L. Bolinger, H. Manos, et al., 31P nuclear magnetic resonance spectroscopic investigation of human neuroblastoma in situ, N. Engl. J. Med. 312 (1985) 1500-1505.
[34] W. Lin, G. Arthur, Phospholipids are synthesized in the G2/M phase of the cell cycle, Int. J. Biochem. Cell Biol. 39 (2007) 597-605.
[35] D.G. Deavall, E.A. Martin, J.M. Horner, R. Roberts, Drug-induced oxidative stress and toxicity, J. Toxicol. 2012 (2012) 645460.
[36] J. Klawitter, J. Gurshtein, K. Corby, S. Fong, M. Tagliaferri, L. Quattrochi, et al., Bezielle (BZL101)-induced oxidative stress damage followed by redistribution of metabolic fluxes in breast cancer cells: a combined proteomic and metabolomic study, Int. J. Cancer. 129 (2011) 2945-2957.
[37] J.S. Kim, E.J. Kim, H.J. Kim, J.Y. Yang, G.S. Hwang, C.W. Kim, Proteomic and metabolomic analysis of H2O2-induced premature senescent human mesenchymal stem cells, Exp. Gerontol. 46 (2011) 500-510.
[38] J. Zeng, J. Liu, G.Y. Yang, M.J. Kelly, T.L. James, L. Litt, Exogenous ethyl pyruvate versus pyruvate during metabolic recovery after oxidative stress in neonatal rat cerebrocortical slices, Anesthesiology. 107 (2007) 630-640.
[39] G. Minotti, P. Menna, E. Salvatorelli, G. Cairo, L. Gianni, Anthracyclines: molecular advances and pharmacologic developments in antitumor activity and cardiotoxicity, Pharmacol. Rev. 56 (2004) 185-229.
[40] L. Roca-Alonso, L. Pellegrino, L. Castellano, J. Stebbing, Breast cancer treatment and adverse cardiac events: what are the molecular mechanisms?, Cardiology. 122 (2012) 253-259.
[41] D. Han, M. Shinohara, M.D. Ybanez, B. Saberi, N. Kaplowitz, Signal transduction pathways involved in drug-induced liver injury, Handb. Exp. Pharmacol. (2010) 267-310.

[42] P. Bhaiya, S. Roychowdhury, P.M. Vyas, M.A. Doll, D.W. Hein, C.K. Svensson, Bioactivation, protein haptenation, and toxicity of sulfamethoxazole and dapsone in normal human dermal fibroblasts, Toxicol. Appl. Pharmacol. 215 (2006) 158-167.
[43] R. Duncan, Y.N. Sat-Klopsch, A.M. Burger, M.C. Bibby, H.H. Fiebig, E.A. Sausville, Validation of tumour models for use in anticancer nanomedicine evaluation: the EPR effect and cathepsin B-mediated drug release rate, Cancer Chemother. Pharmacol. 72 (2013) 417-427.
[44] V.J. Bouchard, M. Rouleau, G.G. Poirier, PARP-1, a determinant of cell survival in response to DNA damage, Exp. Hematol. 31 (2003) 446-454.
[45] A. Skladanowski, J. Konopa, Adriamycin and daunomycin induce programmed cell death (apoptosis) in tumour cells, Biochem. Pharmacol. 46 (1993) 375-382.
[46] J.M. Hakumaki, H. Poptani, A.M. Sandmair, S. Yla-Herttuala, R.A. Kauppinen, 1H MRS detects polyunsaturated fatty acid accumulation during gene therapy of glioma: implications for the in vivo detection of apoptosis, Nat. Med. 5 (1999) 1323-1327.
[47] R.C. Crain, R.W. Clark, B.E. Harvey, Role of lipid transfer proteins in the abnormal lipid content of Morris hepatoma mitochondria and microsomes, Cancer Res. 43 (1983) 3197-3202.
[48] J.L. Griffin, C. Blenkiron, P.K. Valonen, C. Caldas, R.A. Kauppinen, High-resolution magic angle spinning 1H NMR spectroscopy and reverse transcription-PCR analysis of apoptosis in a rat glioma, Anal. Chem. 78 (2006) 1546-1552.
[49] S. Tiziani, A. Lodi, F.L. Khanim, M.R. Viant, C.M. Bunce, U.L. Gunther, Metabolomic profiling of drug responses in acute myeloid leukaemia cell lines, PLoS One. 4 (2009) e4251.
[50] N.W. Lutz, M.E. Tome, P.J. Cozzone, Early changes in glucose and phospholipid metabolism following apoptosis induction by IFN-gamma/TNF-alpha in HT-29 cells, FEBS Lett. 544 (2003) 123-128.
[51] K.E. van der Vos, P. Eliasson, T. Proikas-Cezanne, S.J. Vervoort, R. van Boxtel, M. Putker, et al., Modulation of glutamine metabolism by the PI(3)K-PKB-FOXO network regulates autophagy, Nat. Cell Biol. 14 (2012) 829-837.
[52] D. Dutta, J. Xu, M.L. Dirain, C. Leeuwenburgh, Calorie restriction combined with resveratrol induces autophagy and protects 26-month-old rat hearts from doxorubicin-induced toxicity, Free Radic Biol Med. 74 (2014) 252-262.

Figures

Figure 1

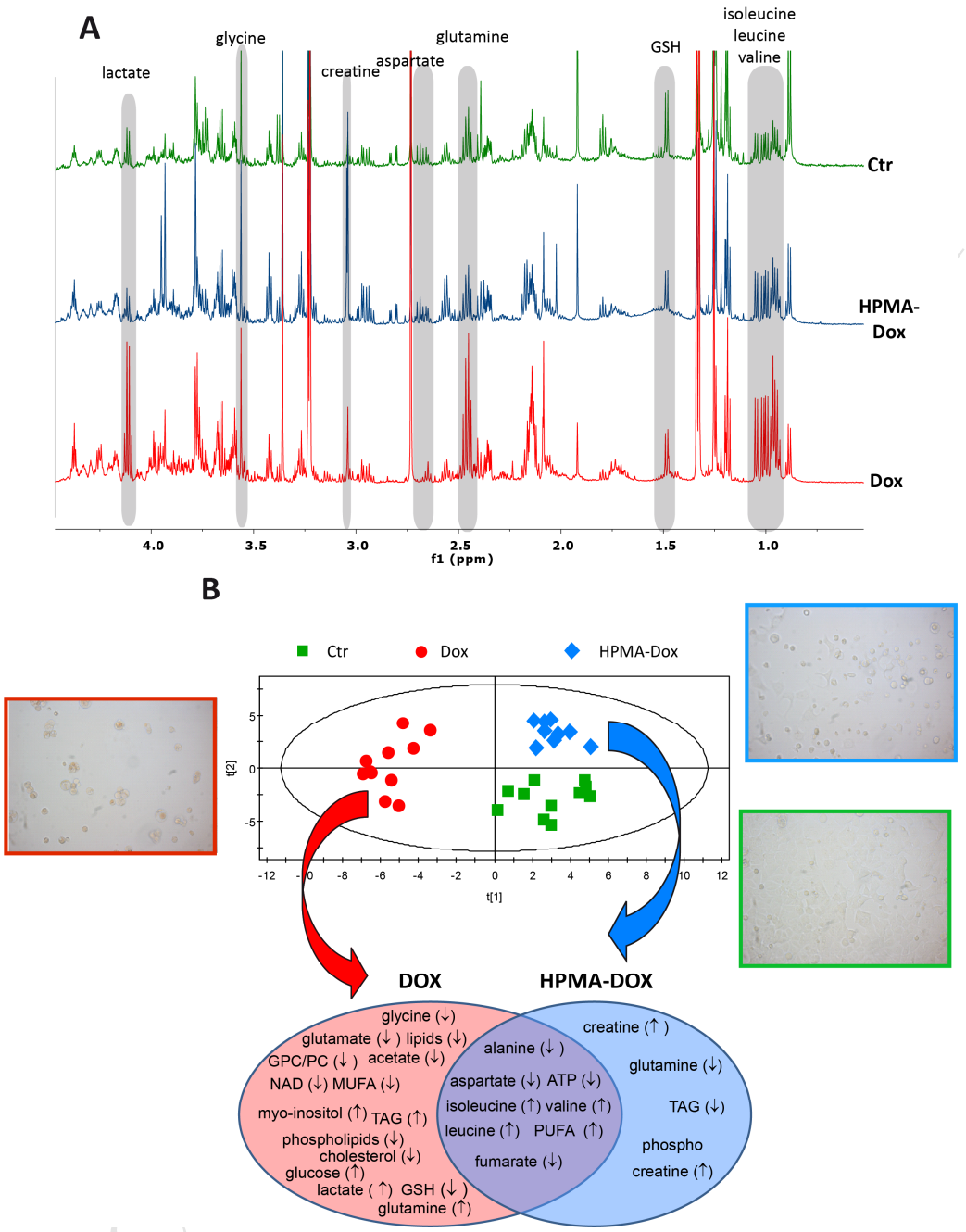

Figure 2

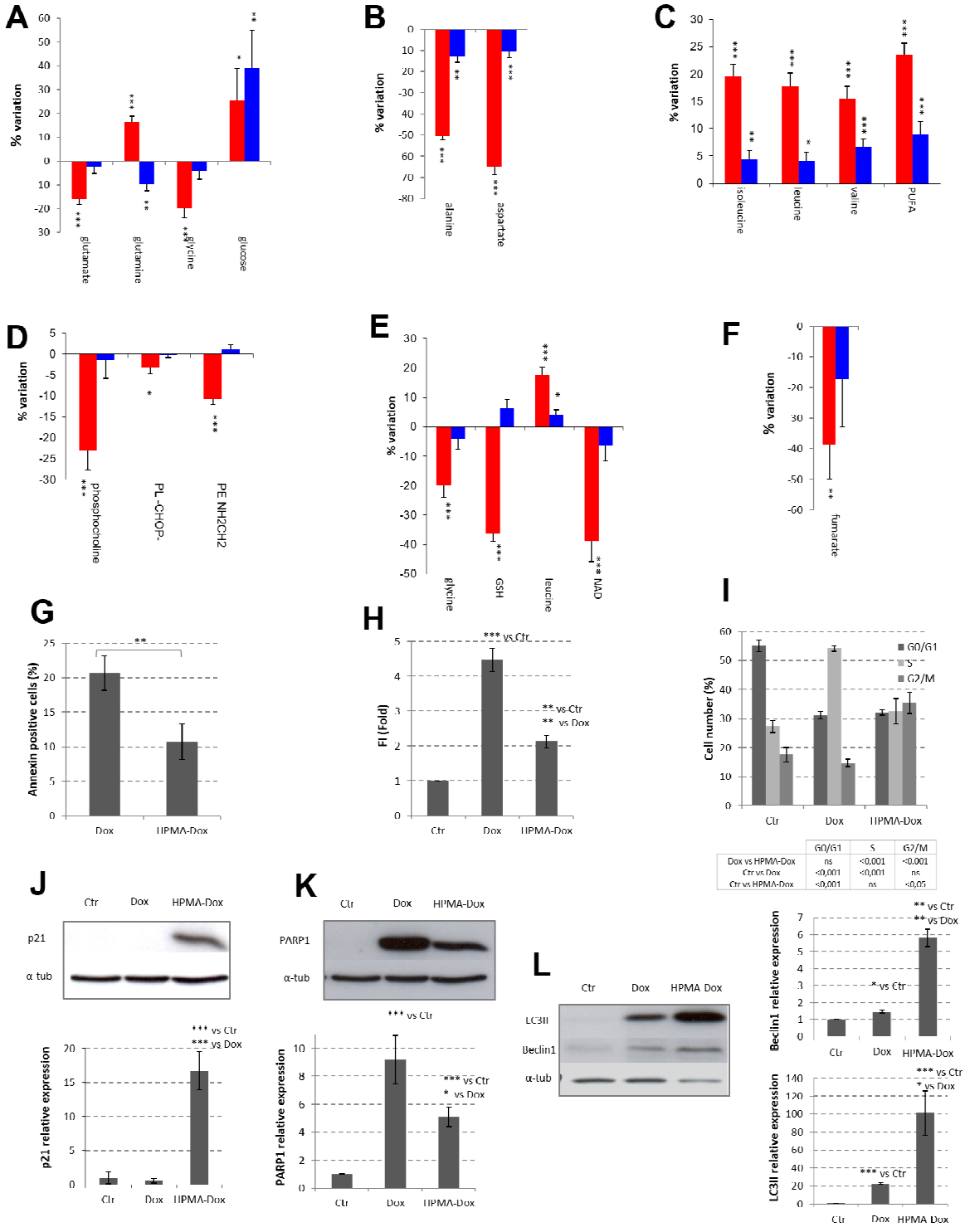
A
% variation
glutamate
glutamine
glycine
glucose
B
% variation
alanine
aspartate
C
% variation
isoleucine
leucine
valine
PUFA
D
% variation
phosphocholine
PL-CHOP-
PE NH2CH2
E
% variation
glycine
GSH
leucine
NAD
F
% variation
fumarate
G
Annexin positive cells (%)
Dox
HPMA-Dox
H
FI (Fold)
*** vs Ctr
** vs Ctr
** vs Dox
Ctr
Dox
HPMA-Dox
I
Cell number (%)
G0/G1
S
G2/M
Ctr
Dox
HPMA-Dox
G0/G1 S G2/M
Dox vs HPMA-Dox ns <0,001 <0,001
Ctr vs Dox <0,001 <0,001 ns
Ctr vs HPMA-Dox <0,001 ns <0,05
J
Ctr
Dox
HPMA-Dox
p21
α tub
p21 relative expression
*** vs Ctr
*** vs Dox
K
Ctr
Dox
HPMA-Dox
PARP1
α-tub
PARP1 relative expression
*** vs Ctr
*** vs Ctr
* vs Dox
L
Ctr
Dox
HPMA Dox
LC3II
Beclin1
α-tub
Beclin1 relative expression
** vs Ctr
** vs Dox
* vs Ctr
LC3II relative expression
*** vs Ctr
* vs Dox
*** vs Ctr

Figure 3

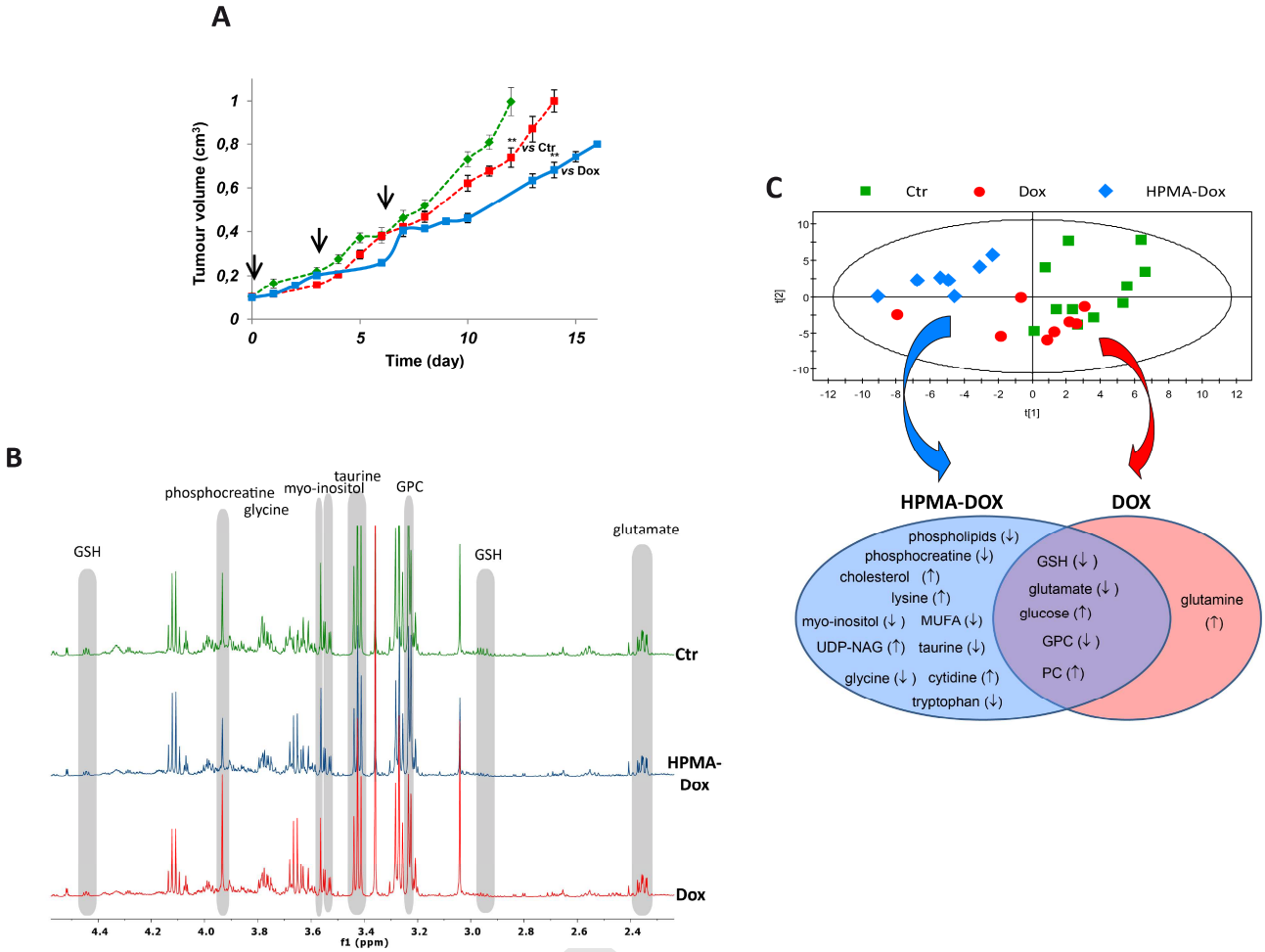

Figure 4

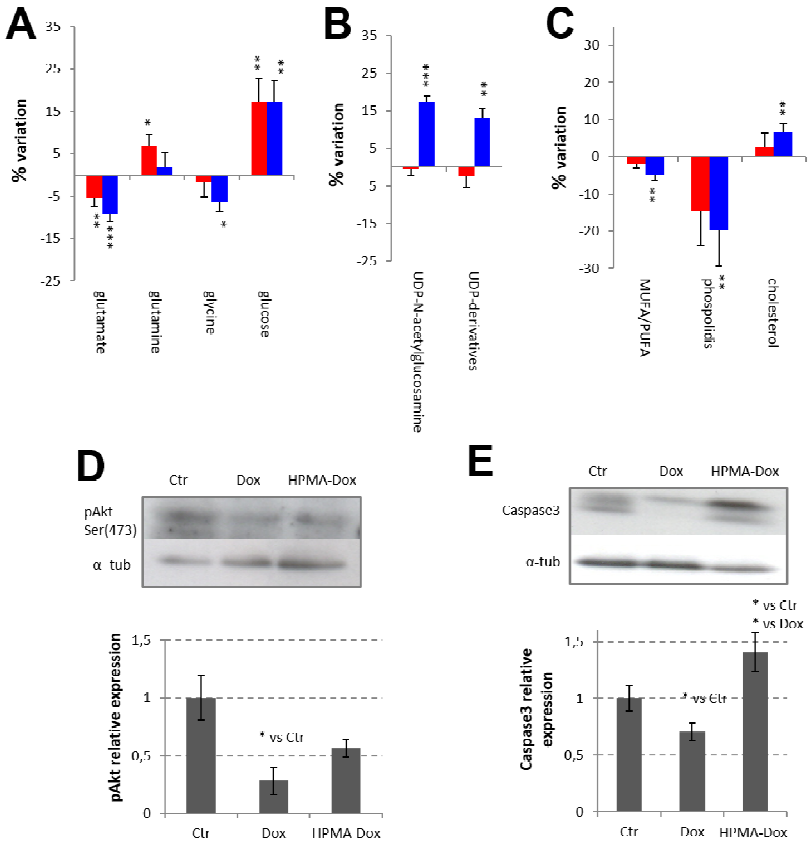

Figure Legends

Figure 1. Metabolomics analysis of MCF7 cells treated with free Dox or HPMA-Dox. A, representative ^{1}H NMR spectra of the aqueous extract corresponding to untreated MCF7 cells, and cells treated with Dox or HPMA-Dox. Spectra were acquired at 27 ºC and 600 MHz. B, PCA score plot (R2X(cum) = 0.63, Q2(cum) = 0.53, UV scaling) obtained from metabolomics data of the three groups (Ctr, HPMA-Dox, Dox). Microscopy images (20x magnification) of MCF7 cell cultures under the different experimental conditions are also shown. Metabolites responsible for the separation of the different groups are summarized using a Venn diagram.

Figure 2. Characterization of metabolite, protein expression, and cell cycle profiles of MCF7 cells after treatment with HPMA-Dox or free Dox. Variations (%) between control cells and Dox treated cells (red bars) or HPMA-Dox (blue bars) treated cells in the levels of metabolites associated with: glycolysis and glutaminolysis (A), alanine and aspartate metabolism (B), apoptosis (C), metabolism of phospholipids (D), oxidative stress (E) and fumarate (F) of Dox and HPMA-Dox treated MCF7 cells compared to untreated cells. Results are reported as average ± SEM. (n=9). **(**G), levels of apoptosis after treating MCF7 cells with Dox and HPMA-Dox at 7.5 µg/ml Dox equiv. for 72 h. Cells were stained with AnnexinV and the results are shown as the percentage of positive cells for staining. (H), fluorescence intensity associated with ROS levels using DCFH-DA and flow cytometry.(I), effects of Dox and HPMA-Dox on the cell cycle of MCF7 cells based on PI staining by flow cytometry. Results are shown as average ± SEM (n > 3). Evaluation of the expression of p21 (J), PARP-1(K) and proteins associated with autophagy (L) (LC3II and Beclin1) in MCF7 cell cultures after treatments. Densitometry analysis is reported as average ± SEM (n = 3). Representative Western blot images are also shown in the figure. (*p<0.05, **p<0.01, ***p <0.001).

Figure 3. Metabolomics analysis corresponding to the analysis of an orthotopic breast tumor mouse model following treatment with Dox or HPMA-Dox. A, Evaluation of the anti-tumor activity of Dox and HPMA-Dox. Treatments were administered at 3 mg/kg and injected 3 times every 3 days. Results are expressed as average ± SEM (n = 7; ** p< 0.01). Green, red and blue colors represent control (Ctr) animals, and Dox or HPMA-Dox treated animals, respectively. Arrows represent day of injection. B, representative ^{1}H NMR spectra of the aqueous extract of untreated tumors and tumors treated with Dox and HPMA-Dox. Spectra were acquired at 27 ºC and 600 MHz. C, OPLS-DA score plot corresponding to the three groups (R2Y(cum) 0.62, Q2(cum) = 0.33, UV scaling). Metabolites responsible for the separation of the different groups are summarized using a Venn diagram.

Figure 4. Impact of the treatment with Dox or HPMA-Dox in the metabolite and protein expression profile of an orthotopic breast tumor mouse model. A, Variations (%) between control animals and Dox treated animals (red bars) or HPMA-Dox treated animals (blue bars) in the levels of metabolites associated with glycolysis and glutaminolysis (A), apoptosis (B) and lipid metabolism (C) measured in mice tumors after treatment with Dox and HPMA-Dox. Results are shown as average ± SEM (n=7). (D) and (E), pAkt (Ser473) and caspase-3 expression levels, respectively, in the presence of Dox and HPMA-Dox, as measured by western blot in tumor samples. Protein quantification was performed by densitometry analysis (average ± SEM (n=6)). (*$p<0.05$, **$p<0.01$, ***$p<0.001$).

Supplementary Data

Table S1: Integration regions corresponding to the metabolites identified in the aqueous phase of MCF7 cell extracts.

Table S2: Integration regions corresponding to the metabolites identified in the organic phase of MCF7 cell extracts.

Table S3: Intregration regions corresponding to the metabolites identified in the medium of MCF7 cell cultures.

Table S4: Integration regions corresponding to the metabolites identified in the aqueous phase of tumor extracts.

Table S5: Integration regions corresponding to the metabolites identified in the organic phase of tumor extracts.

Table S6: Abbreviations used in the manuscript.

Scheme S1. Synthetic strategy followed to obtain the HPMA-Dox conjugate. DMF: Dimethylformamide; RT: room temperature; TEA: Triethylenamine; GFLG: Gly-Phe-Leu-Gly; Onp: p-nitrophenol.

Figure S1. Cell viability of MCF7 cells after treatment with HPMA-Dox (A) and free Dox (B). Results are reported as average ± SEM (n =3).

Figure S2. (A) Cell counts after 72h of cell culture of untreated cells (Ctr), free Dox treated cells and HPMA-Dox treated cells. (B) Clonogenic capacity of MCF7 cells after 72 h of incubation with free Dox or HPMA-Dox. Results are represented as average ± SEM.

Figure S3. Representative ^{1}H NMR spectra of the organic phase corresponding to extracts of untreated MCF7 cells, and cells treated with Dox or HPMA-Dox. Spectra were acquired at 27 ºC and 600 MHz.

Figure S4. PCA loadings plot corresponding to the discrimination of untreated MCF7 cells, and cells treated with Dox or HPMA-Dox, based on the aqueous cell extracts.

Figure S5. Variations (%) of metabolite levels corresponding to the aqueous and organic phases of MCF7 cell extracts in the presence of low and high doses of Dox and HPMA-Dox.

Figure S6. Variations (%) in the levels of medium metabolites, corresponding to the comparison between 0 h and 72 h of incubation time, in the absence and presence of low (LD) and high (HD) doses of Dox and HPMA-Dox. Control samples were used to match culture day, medium bottle and dilution (*$p<0.05$).

Figure S7. Evolution of body weight, expressed as a percentage of the initial weight, in untreated (Ctr) and treated animals with Dox and HPMA-Dox.

Figure S8. Representative ^{1}H NMR spectra of the organic phase corresponding to extracts of untreated and treated breast tumors with Dox and HPMA-Dox. Spectra were acquired at 27 ºC and 600 MHz.

Figure S9. A, OPLS-DA score plot corresponding to the comparison of untreated *vs* treated breast tumors with free Dox. R2Y (cum) = 0,68, Q2 (cum) = 0,15. (Permutation test: R2 = 0.53, Q2 = -0.77, cross validation ($p<0.05$)). B, S-plot derived from the OPLS-DA model.

Figure S10. A, OPLS-DA score plot corresponding to the comparison of untreated *vs* treated breast tumors with HPMA-Dox. R2Y (cum) = 0,88, Q2 (cum) = 0,74. (Permutation: R2 = 0. 61, Q2 = -0.47, cross validation test ($p<0.0001$)) B, S-plot derived from the OPLS-DA model.

Figure S11. Variations (%) of metabolite levels corresponding to the aqueous (polar metabolites) and organic (non-polar metabolites) phases of extracts of breast tumors after the administration of Dox and HPMA-Dox.

Figure 1

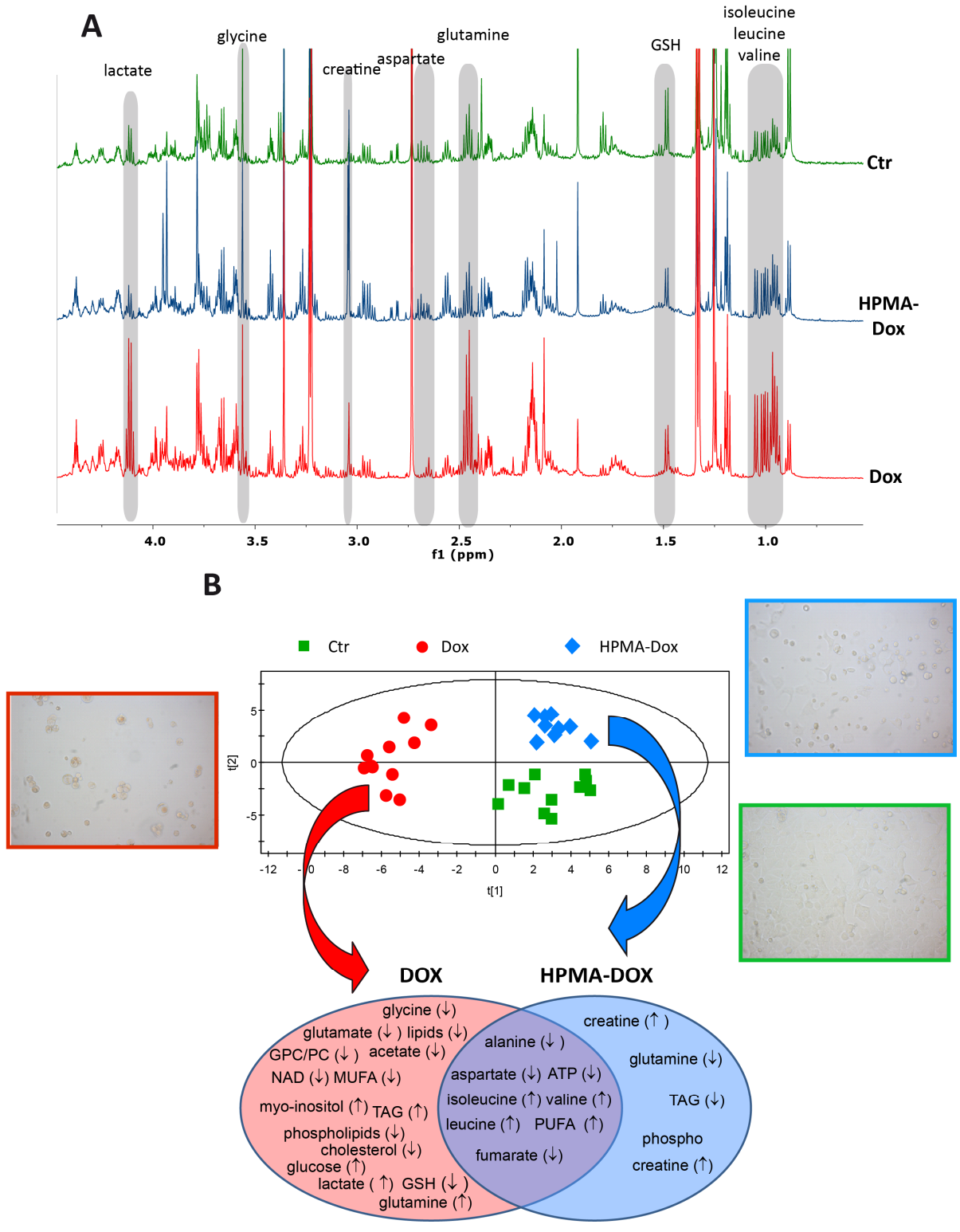
A
lactate
glycine
creatine
aspartate
glutamine
GSH
isoleucine
leucine
valine
Ctr
HPMA-Dox
Dox
4.0
3.5
3.0
2.5
2.0
1.5
1.0
f1 (ppm)
B
Ctr
Dox
HPMA-Dox
t[1]
t[2]
DOX
HPMA-DOX
glycine (↓)
glutamate (↓) lipids (↓)
GPC/PC (↓) acetate (↓)
NAD (↓) MUFA (↓)
myo-inositol (↑) TAG (↑)
phospholipids (↓)
cholesterol (↓)
glucose (↑)
lactate (↑) GSH (↓)
glutamine (↑)
alanine (↓)
aspartate (↓) ATP (↓)
isoleucine (↑) valine (↑)
leucine (↑) PUFA (↑)
fumarate (↓)
creatine (↑)
glutamine (↓)
TAG (↓)
phospho
creatine (↑)

Figure 2

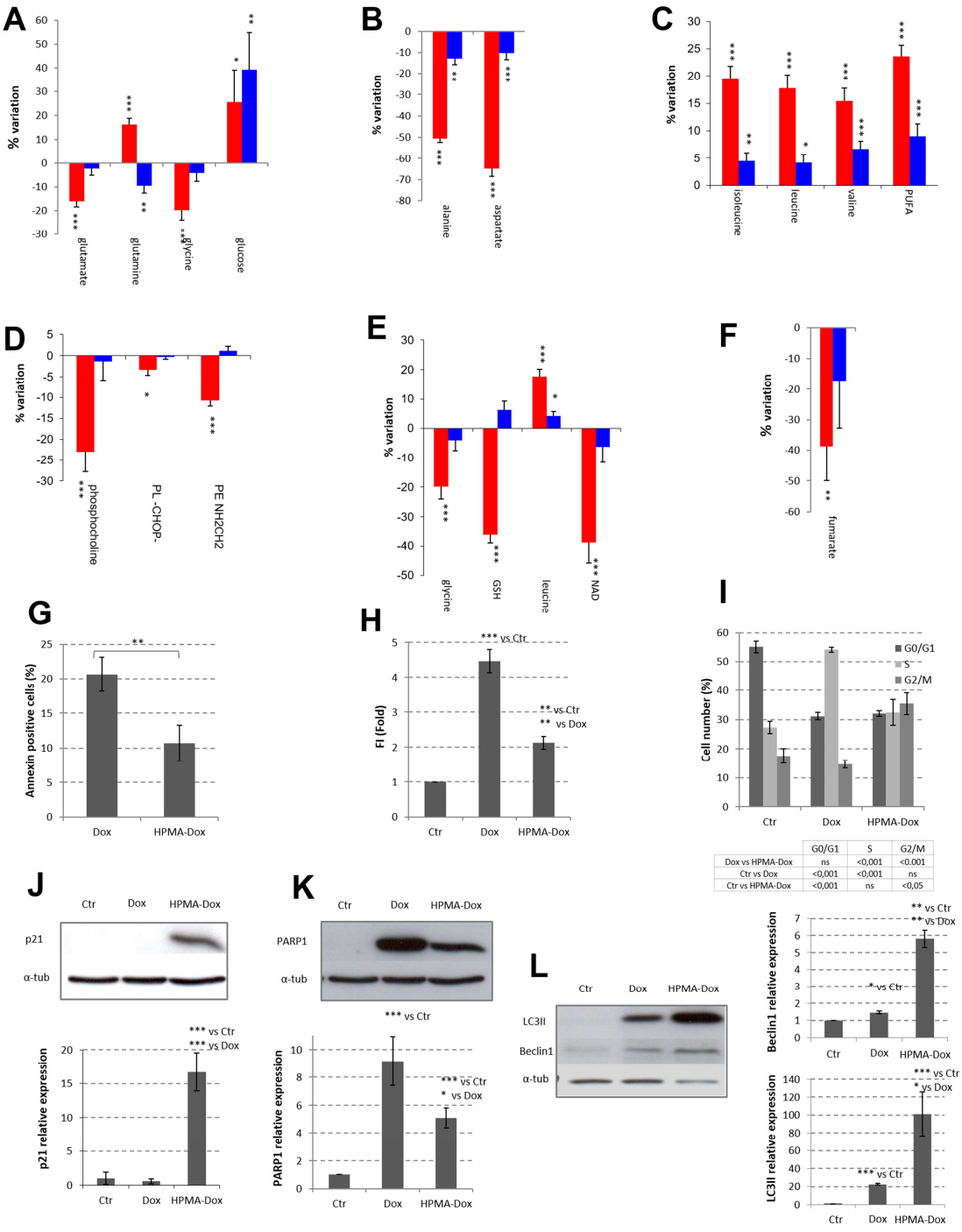
A
% variation
glutamate
glutamine
glycine
glucose
B
% variation
alanine
aspartate
C
% variation
isoleucine
leucine
valine
PUFA
D
% variation
phosphocholine
PL -CHOP-
PE NH2CH2
E
% variation
glycine
GSH
leucine
NAD
F
% variation
fumarate
G
Annexin positive cells (%)
Dox
HPMA-Dox
H
FI (Fold)
*** vs Ctr
** vs Ctr
** vs Dox
Ctr
Dox
HPMA-Dox
I
Cell number (%)
G0/G1
S
G2/M
Ctr
Dox
HPMA-Dox
G0/G1 S G2/M
Dox vs HPMA-Dox ns <0,001 <0.001
Ctr vs Dox <0,001 <0,001 ns
Ctr vs HPMA-Dox <0,001 ns <0,05
J
Ctr
Dox
HPMA-Dox
p21
α-tub
p21 relative expression
*** vs Ctr
*** vs Dox
K
Ctr
Dox
HPMA-Dox
PARP1
α-tub
*** vs Ctr
PARP1 relative expression
*** vs Ctr
* vs Dox
L
Ctr
Dox
HPMA-Dox
LC3II
Beclin1
α-tub
Beclin1 relative expression
** vs Ctr
** vs Dox
* vs Ctr
LC3II relative expression
*** vs Ctr
* vs Dox
*** vs Ctr

Figure 3

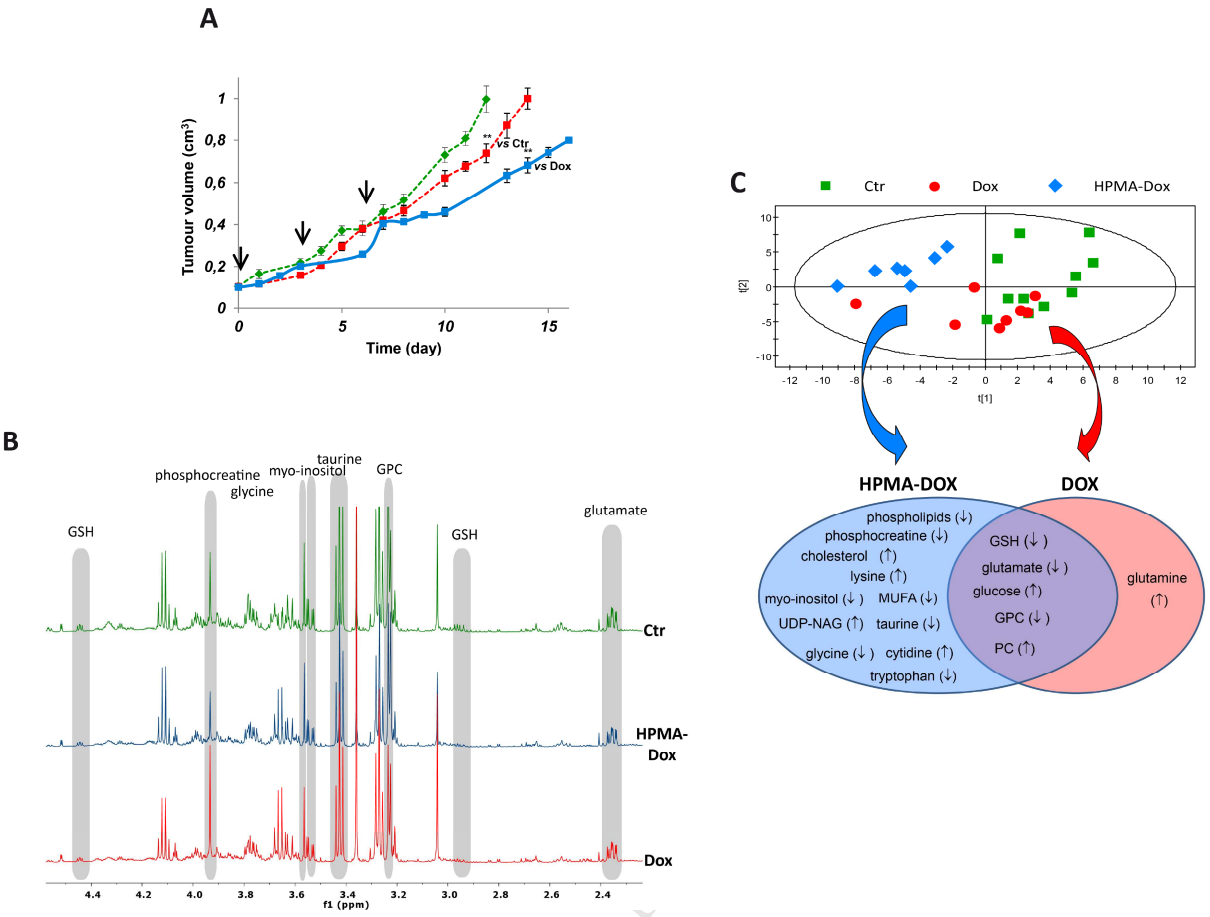

Figure 4

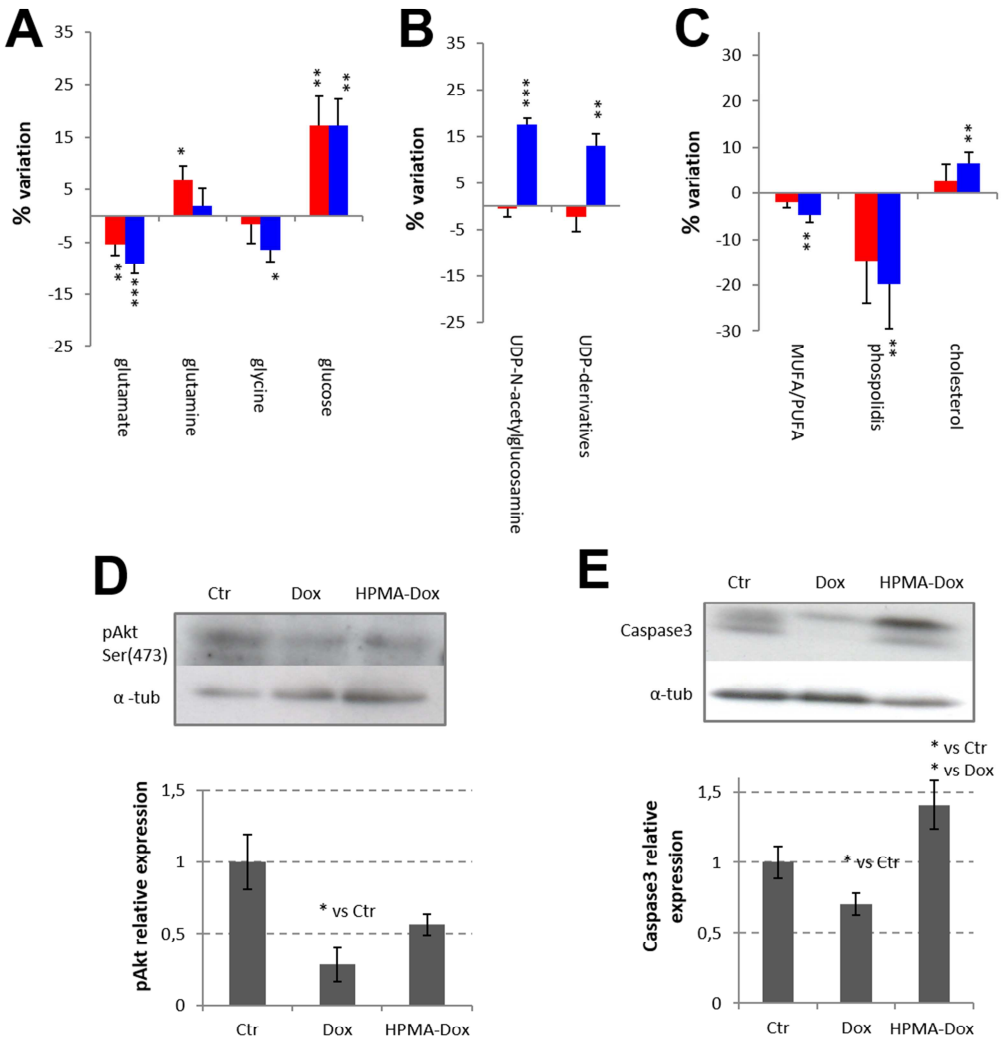
A
% variation
glutamate
glutamine
glycine
glucose
B
% variation
UDP-N-acetylglucosamine
UDP-derivatives
C
% variation
MUFA/PUFA
phospolidis
cholesterol
D
Ctr
Dox
HPMA-Dox
pAkt Ser(473)
α -tub
pAkt relative expression
* vs Ctr
E
Caspase3
α-tub
Caspase3 relative expression
* vs Ctr
* vs Dox